Accepted Manuscript

A fast numerical algorithm for a basic dual integral equation of the flapping wing in a flow of non-viscous incompressible fluid

V.V. Popuzin, M.A. Sumbatyan, A.E. Tarasov

PII: S0377-0427(18)30331-5
DOI: https://doi.org/10.1016/j.cam.2018.05.054
Reference: CAM 11719

To appear in: *Journal of Computational and Applied Mathematics*

Received date : 23 May 2016
Revised date : 29 April 2018

Please cite this article as: V.V. Popuzin, M.A. Sumbatyan, A.E. Tarasov, A fast numerical algorithm for a basic dual integral equation of the flapping wing in a flow of non-viscous incompressible fluid, *Journal of Computational and Applied Mathematics* (2018), https://doi.org/10.1016/j.cam.2018.05.054

A Fast Numerical Algorithm for a Basic Dual Integral Equation of the Flapping Wing in a Flow of Non-Viscous Incompressible Fluid

V.V. Popuzin, M.A. Sumbatyan, A.E. Tarasov
Institute of Mathematics, Mechanics and Computer Science,
Southern Federal University,
Milchakova Street 8a, 344090 Rostov-on-Don, Russia
e-mail: popuzin@gmail.com, sumbat@math.rsu.ru, tarasovmech@gmail.com

Abstract

The present paper proposes a new approach to the classical problem of the harmonic oscillations of a thin wing in a flow of non-viscous incompressible fluid. The problem is reduced to a dual integral equation, permitting application of numerical methods. The numerical experiments are performed by using some advanced fast non-stationary iterative methods, with the help of the two-dimensional Fast Fourier Transform. There is given a brief survey on the iterative methods, to evaluate the most efficient algorithms in application to the considered problem of the flapping wing theory.

Key words: flapping wing; dual integral equation; numerical algorithm; Toeplitz blocks; conjugate gradients; bi-conjugate gradients

1 Introduction

The aerohydrodynamics of birds' flight and swimming of fishes and dolphins was a subject of a very intensive investigation since the beginning of the 20th century, a historical survey on the mathematical simulation is presented in [1]. Among recent

works, let us cite those on applications to the flight theory in bionics [2–6]. However, reproduction of outer characteristics of motion of biological individual cannot give complete understanding of the motion work. This in fact requires an adequate mathematical analysis. That is why some fundamental methods were developed based on computer simulation. Since the basic property of the unsteady flow around bodies is generation of vortex wakes, one of classical approaches is connected with the vortex element method, well developed in various versions [7–10]. Some aerodynamic theories for flexible airfoils and wings are discussed in [11–17]. In particular cases these theories give classical predictions known for rigid airfoils. At last, it should be noted that there are several commercial programs which permit numerical study of the problem under consideration. In the 3d case commercial programs require, as a rule, very huge computer resources.

Within the model of incompressible and non-viscous fluid, in the case of wing placed in a uniform stream and harmonically oscillating in time, the 3d problem can be reduced to a dual integral equation which is an expansion of the classical integral equation, known in the lifting surface theory, to the non-stationary problem [18]. Many approximate analytical and numerical approaches have been proposed to solve this dual integral equation. In particular, efficient asymptotic techniques can be applied to the cases of large and small aspect ratio of the wing. However, the answer to the question about appropriate algorithms, which can provide the desired precision in real time, is still unclear. The mesh reduction method under consideration leads to the dual integral equation in the 3d theory, hence this reduces significantly the size of the mesh. Nevertheless a dense system of nodes distributed over the two-dimensional domain generates a fully populated matrix of too huge dimension, to be practicable when implemented on personal computers.

In [19] the authors apply a fast algorithm to a simpler dual integral equation. Physically, the used characteristic hyper-singular kernel arises in the 3d problem of harmonic oscillations of the wing in the motionless fluid, under conditions of a linear theory of small perturbations. This problem is therefore a particular case of the present study if the velocity of the incoming stream is equal to zero. In this particular case the kernel of the integral equation can be calculated explicitly, which in fact turns out a characteristic hyper-singular kernel of two variables. Furthermore, the discretization process with a two-dimensional rectangular grid leads to a matrix with double symmetry and all real eigenvalues. The fast algorithm proposed in [19] is based on the idea of iterative

construction of the inverse matrix via a certain variation of the Newton's method applied in the matrix form, namely the Newton-Hotelling-Schulze's method. The authors use an advanced numerical technique of the data compression and data partitioning, to speed-up the matrix inversion process. For this purpose they apply such non-linear approximations as wavelets, low-rank and tensor approaches. The obtained inverse matrix can be multiplied by the right-hand side, to calculate the unknown vector. This can also be used as a preconditioner in some non-stationary iterative algorithms.

In contrast to the simple integral equation with the characteristic kernel described in the previous paragraph, the kernel arising in the problem at hand cannot be calculated in explicit form. Therefore, this requires a special treatment, to provide its efficient numerical calculation. So far as an appropriate numerical treatment of the kernel is arranged, the fast numerical algorithm to find the solution can be constructed in the way allied to [19]. **In particular, in the present work the well-known approach of the iterative solver with a two-dimensional circulant preconditioner is used [20, 21], to provide efficient solution.**

In section 2 we give a physical formulation of the problem and reduce the corresponding boundary value problem to a basic dual integral equation. In section 3 we present an analytical treatment for the kernel of the initial integral equation to the form, suitable to apply an efficient numerical scheme. In section 4 we perform a discretization of the dual integral equation, reducing it to a System of Linear Algebraic Equations (SLAE). Sections 5 and 6 cover some **modern** approaches to improve the efficiency of the applied algorithms, namely, a FFT-based matrix-vector multiplication and a preconditioning technique [22–25]. Finally, some numerical experiments and conclusions are given in the last two sections.

2 Problem Formulation and the Basic Dual Integral Equation

Let a thin wing of the size $(-\ell, \ell)\times(-c, c)$, rectangular in plan, be placed into a uniform stream of non-viscous incompressible fluid, see Fig. 1. The velocity vector of the incoming flow is constant and directed along axis x: $\bar{v} = \{u_0, 0, 0\}$. We assume that the oscillations of the wing are harmonic in time, therefore, in the linear aerodynamic theory all physical quantities in the perturbed motion have the following form: $\tilde{F}(x, y, z, t) = \mathrm{Re}[F(x, y, z)\exp(-i\omega t)]$. Let function $z = \tilde{W}(x, y, t) = \mathrm{Re}[W(x, y)\exp(-i\omega t)]$ define

the shape of the wing.

If the fluid is incompressible and the motion is potential (vortex-free) then the continuity equation implies

$$\operatorname{div}\bar{v}=0, \qquad \bar{v}=\operatorname{grad}\varphi, \implies \Delta\varphi=0. \tag{1}$$

Once the potential φ is known, the aerodynamic pressure can be determined from the Lagrange-Cauchy integral:

$$\frac{\partial\tilde{\varphi}}{\partial t}+\frac{\tilde{p}}{\rho}+\frac{\tilde{v}^2}{2}=F(t), \tag{2}$$

where ρ is the mass density of the fluid.

In frames of the linear aerodynamic theory we assume that:

(i) the wing is an absolutely thin plate which is weakly curved and weakly inclined with respect to direction of incidence, axis x.

(ii) the added perturbations of velocity and pressure caused by the oscillations of the plate are asymptotically small when compared, respectively, with the velocity and the pressure in the incoming flow. If any perturbed quantity is marked by an accent sign, then this hypothesis implies:

$$\bar{v}=\bar{u}_0+\bar{v}', \quad (|v'|/u_0\ll 1), \qquad p=p_0+p', \quad (|p'|/p_0\ll 1), \qquad \varphi=\varphi_0+\varphi'. \tag{3}$$

By substituting expressions (3) into Eq. (2) and keeping only linear terms for all perturbed quantities, one obtains:

$$\begin{gathered} v_x=u_0+v_x',\ v_y=v_y',\ v_z=v_z', \implies \frac{\partial\tilde{\varphi}}{\partial t}+\frac{\tilde{p}}{\rho}+u_0\,\tilde{v}_x=F(t), \\ \implies \frac{p'}{\rho}+u_0\,v_x'-i\omega\varphi'=0\,, \implies \frac{p'}{\rho}+u_0\,\frac{\partial\varphi'}{\partial x}-i\omega\varphi'=0\,. \end{gathered} \tag{4}$$

Let the wing be defined by the equation $z=W(x,y)$ which is in fact a complex amplitude in the time-harmonic regime. Then the slip boundary condition over the wing surface is

$$v_z|_S=\frac{dW}{dt} \implies v_z'|_S=\frac{\partial W}{\partial t}+(u_0+v_x')\frac{\partial W}{\partial x}+v_y'\frac{\partial W}{\partial y}+v_z'\frac{\partial W}{\partial z}\,. \tag{5}$$

It follows from hypothesis (i) above that $|\partial f/\partial x|\ll 1$, $|\partial f/\partial y|\ll 1$. Then, in the linear approximation, for the process harmonic in time, boundary condition (5) can be rewritten in the following form:

$$v_z'|_S=u_0\,\frac{\partial W}{\partial x}-i\omega W\,, \implies \left.\frac{\partial\varphi'}{\partial z}\right|_S=u_0\,\frac{\partial W}{\partial x}-i\omega W\,. \tag{6}$$

The last hypothesis of the linearized aerodynamic theory is applied as follows:

(iii) the slip boundary condition (6) may be satisfied on projection of domain S to the horizontal plane xy, instead of the true curved surface.

Therefore, in the forthcoming discussions we imply that domain S is a plane rectangular domain $S = (-\ell, \ell) \times (-c, c)$, a certain subset of the plane xy.

Let us consider the full space, filled of the fluid, separately for $z > 0$ and $z < 0$, where all physical quantities will be marked by $+$ or $-$, respectively. The interface plane $z = 0$ is a union of domain S, a certain vortex sheet which is carried away to $x \to +\infty$ by the flow, and the rest domain where all physical quantities should be continuous when crossing plane $z = 0$.

It is clear from Eq. (4) that if function φ' is harmonic then function p' is harmonic too: $\Delta p' = 0$. Application of the double Fourier transform with respect to variables x and y reduces the Laplace equation for function p' to the ordinary differential equation regarding variable z:

$$P(\alpha, \beta, z) = \iint_{-\infty}^{\infty} p'(x, y, z) e^{i(\alpha x + \beta y)} d\alpha d\beta, \quad \frac{\partial^2 P}{\partial z^2} - (\alpha^2 + \beta^2) P = 0, \tag{7}$$

whose solution is

$$P_{\pm}(\alpha, \beta, z) = A_{\pm}(\alpha, \beta) e^{\mp rz}, \qquad r(\alpha, \beta) = (\alpha^2 + \beta^2)^{1/2}. \tag{8}$$

Since boundary condition (6) should be valid for both sides of the wing, $z = +0$ and $z = -0$, it follows from (6) that function $\partial\varphi'/\partial z$ is even with respect to variable z, hence function φ' is odd with respect to z. Then one can conclude from Eq. (4) that function p' is odd with respect to z. This implies

$$\begin{gathered} P_{\pm}(\alpha, \beta, z) = \pm A(\alpha, \beta) e^{\mp rz}, \implies \\ p'_{\pm}(x, y, z) = \pm \frac{1}{4\pi^2} \iint_{-\infty}^{\infty} A(\alpha, \beta) e^{-i(\alpha x + \beta y) \mp rz} \, d\alpha d\beta. \end{gathered} \tag{9}$$

Let us introduce the new unknown function $\gamma(x, y)$, as follows:

$$p'_{+}(x, y, +0) = \frac{1}{2} \left[p'_{+}(x, y, +0) - p'_{-}(x, y, -0) \right] = \begin{cases} \gamma(x, y), & (x, y) \in S, \\ 0, & (x, y) \notin S. \end{cases} \tag{10}$$

The trivial value of this function outside domain S, occupied by the wing, follows from the continuity of aerodynamic pressure outside the wing.

It should be noted that physical meaning of the introduced function γ directly follows from relation (10): this is half the difference between the values of aerodynamic pressure above and below the wing.

It is evident from (9) and (10) that

$$A(\alpha,\beta)=\iint_{-\infty}^{\infty}\gamma(\xi,\eta)e^{i(\alpha\xi+\beta\eta)}d\xi d\eta=\iint_{S}\gamma(\xi,\eta)e^{i(\alpha\xi+\beta\eta)}d\xi d\eta. \tag{11}$$

Now, by substituting Eq. (11) to Eq. (9), one finally obtains the expression for aerodynamic pressure in terms of the introduced function γ:

$$p'_{\pm}(x,y,z)=\pm\frac{1}{4\pi^2}\iint_{S}\gamma(\xi,\eta)d\xi d\eta\iint_{-\infty}^{\infty}e^{i[\alpha(\xi-x)+\beta(\eta-y)]\mp rz}\,d\alpha d\beta. \tag{12}$$

Keeping this relation in mind, in order to express the potential φ in terms of function γ, one should inverse relation (4) relatively function φ. This can formally be considered as a partial differential equation regarding function φ. Under the condition of no perturbation when moving to infinity upstream, its solution tending to zero as $x\to-\infty$ can easily be resolved by a standard mathematical method, to give

$$\begin{gathered}\varphi'_{\pm}(x,y,z)=-\frac{1}{\rho u_0}\int_{-\infty}^{x}e^{i\omega(x-\zeta)/u_0}p'_{\pm}(\zeta,y,z)d\zeta=\\ =\pm\frac{1}{4\pi^2\rho}\iint_{S}\gamma(\xi,\eta)d\xi d\eta\iint_{-\infty}^{\infty}\frac{e^{i[\alpha(\xi-\zeta)+\beta(\eta-y)+\omega(x-\zeta)/u_0]\mp rz}}{i(u_0\alpha+\omega)}\,d\alpha d\beta\Bigg|_{\zeta=-\infty}^{x},\end{gathered} \tag{13}$$

where the Cauchy-type singularity at point $\alpha=-\omega/u_0$ is taken as a principal-value singular integral. The key point here is to calculate the limit as $\zeta\to-\infty$:

$$\begin{gathered}\int_{-\infty}^{\infty}\frac{e^{i\alpha(\xi-\zeta)}d\alpha}{i(u_0\alpha+\omega)}=\frac{e^{-i\omega(\xi-\zeta)/u_0}}{u_0}\int_{-\infty}^{\infty}\frac{e^{i[(\alpha+\omega/u_0)(\xi-\zeta)]}}{i(\alpha+\omega/u_0)}d\alpha=\\ =\frac{e^{-i\omega(\xi-\zeta)/u_0}}{u_0}\int_{-\infty}^{\infty}\frac{e^{-i\alpha\zeta}}{i\alpha}d\alpha=-\frac{2e^{-i\omega(\xi-\zeta)/u_0}}{u_0}\int_{0}^{\infty}\frac{\sin(\alpha\zeta)}{\alpha}d\alpha=\\ =-\frac{2e^{-i\omega(\xi-\zeta)/u_0}}{u_0}\,\frac{\pi}{2}\,\mathrm{sign}(\zeta)=-\frac{\pi e^{-i\omega(\xi-\zeta)/u_0}}{u_0}\,\mathrm{sign}(\zeta)\to\frac{\pi}{u_0}\,e^{-i\omega(\xi-\zeta)/u_0}.\end{gathered} \tag{14}$$

Therefore, representation (13) takes the following form:

$$\varphi'_{\pm}(x,y,z)=\pm\frac{1}{4\pi^2\rho u_0}\iint_{S}K_{\varphi}^{\pm}(\xi-x,\eta-y,z)\gamma(\xi,\eta)d\xi d\eta\,, \tag{15a}$$

where $(\mu=\omega/u_0)$

$$K_{\varphi}^{\pm}(\xi,\eta,z)=\iint_{-\infty}^{\infty}\frac{e^{i(\alpha\xi+\beta\eta)\mp r(\alpha,\beta)z}}{i(\alpha+\mu)}\,d\alpha d\beta\;-\;\pi e^{-i\mu\xi}\int_{-\infty}^{\infty}e^{i\beta\eta\mp r(\mu,\beta)z}\,d\beta\,. \tag{15b}$$

Now, by satisfying the boundary condition (6), one can easily derive from (15) the following basic dual integral equation of the problem at hand:

$$\frac{1}{4\pi^2\rho u_0}\iint_S K(\xi-x,\eta-y)\,\gamma(\xi,\eta)d\xi d\eta = i\omega W - u_0\,\frac{\partial W}{\partial x}\,, \tag{16a}$$

with

$$K(\xi,\eta) = \iint_{-\infty}^{\infty}\frac{e^{i(\alpha\xi+\beta\eta)}}{i(\alpha+\mu)}\,r(\alpha,\beta)\,d\alpha d\beta \;-\; \pi e^{-i\mu\xi}\int_{-\infty}^{\infty} e^{i\beta\eta}\,r(\mu,\beta)\,d\beta\,. \tag{16b}$$

Once integral equation (16) is solved by this or that way, all physical characteristics can easily be calculated as some integrals of the basic unknown function $\gamma(x,y)$. For instance, the full aerodynamic force is connected with the dual integral

$$P = \int_{-1}^{1}\int_{-1}^{1}\gamma(x,y)dxdy, \tag{17}$$

and the propulsive thrust, which is the suction force [1], is defined as a limiting value of the single integral:

$$T = \frac{\pi c}{2\rho u_0^2}\lim_{x\to -1}\int_{-\lambda}^{\lambda}|\gamma(x,y)|^2 dy. \tag{18}$$

Therefore, the principal feature of any method applied to this problem is that this should provide fast computations, to construct an efficient solution to the dual integral equation (16). Under the condition that kernel (16b) is itself a dual integral, which cannot be calculated in a closed form, one can easily estimate the number of arithmetic operations required. If a certain grid has N_x nodes along the direction of propagation and N_y nodes in the transversal direction then, taking into account the convolution property of the kernel, one needs to apply $O\left[(N_x\,N_y)^2\right]$ arithmetic operations, only to calculate all elements of a matrix under disretization. After that one needs to solve the matrix equation, which with a direct treatment, say by the Gauss elimination technique, requires $O\left[(N_x\,N_y)^3\right]$ operations. Even in the case $N_x \sim N_y \sim 10^2$, this is of the order $\sim 10^{12}$ which is too huge, at least for personal computers. The main conclusion from this discussion is that any applied numerical algorithm, to be efficient, should be fast. Just this point is the main goal of the present study.

3 Analytical Treatment of the Kernel

Let us rewrite the basic integral equation (15) in the dimensionless form, by

introducing the new variables: $\tilde{x} = x/c,\ \tilde{y} = y/\ell$ **(below tildes are omitted):**

$$\frac{c}{4\pi^2\rho u_0^2}\int_{-1}^{1}\int_{-1}^{1} K(\xi - x, \eta - y)\gamma(\xi,\eta)d\xi d\eta = i\nu W - \frac{\partial W}{\partial x}, \qquad (|x, y| \le 1), \tag{19}$$

where $\nu = \omega c/u_0$ is the Strouhal number, $\lambda = \ell/c$ is the aspect ratio of the wing.

The kernel in Eq. (19) is

$$K(\xi,\eta) = -\frac{\pi e^{-i\nu\xi}}{\lambda} I_1(\eta) + I_2(\xi,\eta), \tag{20}$$

where

$$I_1 = \int_{-\infty}^{\infty} \sqrt{\beta^2 + (\lambda\nu)^2}\, e^{i\beta\eta} d\beta, \quad I_2 = \int_{-\infty}^{\infty} \frac{e^{i\alpha\xi} d\alpha}{i\lambda(\alpha+\nu)} \int_{-\infty}^{\infty} \sqrt{\beta^2 + (\lambda\alpha)^2}\, e^{i\beta\eta} d\beta, \tag{21}$$

and the integral over variable α is treated as the singular Cauchy-type integral, regarding the singularity at the simple pole as $\alpha \to -\nu$.

The first integral in the kernel (21) can be calculated explicitly, by using the value of the tabulated integral [26]:

$$\begin{aligned} I_1(\eta) &= \int_{-\infty}^{\infty} \sqrt{\beta^2 + (\lambda\nu)^2}\, e^{i\beta\eta} d\beta = 2\int_0^{\infty} \sqrt{\beta^2 + (\lambda\nu)^2}\cos(\beta\eta) d\beta = \\ &= -2\lim_{\varepsilon\to+0}\frac{\partial}{\partial\varepsilon}\int_0^{\infty}\cos(\beta\eta)e^{-\varepsilon\sqrt{\beta^2+(\lambda\nu)^2}}d\beta = \\ &= -2\lim_{\varepsilon\to+0}\frac{\partial}{\partial\varepsilon}\frac{\varepsilon\lambda\nu}{\sqrt{\varepsilon^2+\eta^2}}K_1(\lambda\nu\sqrt{\varepsilon^2+\eta^2}) = -2\frac{\lambda\nu}{|\eta|}K_1(\lambda\nu|\eta|), \end{aligned} \tag{22}$$

where K_1 is the Macdonald function [27].

The internal integral in I_2, over variable β, can be calculated by analogy. This permits representation of I_2 as a single integral over variable α:

$$I_2(\xi,\eta) = \int_{-\infty}^{\infty} \frac{e^{i\alpha\xi}}{i\lambda(\alpha+\nu)}\left[-2\frac{\lambda|\alpha|}{|\eta|}K_1(\lambda|\alpha\eta|)\right] d\alpha. \tag{23}$$

The direct numerical calculation of integral (23) is complicated because of irregular behavior of the integrand at the origin and at the infinity. A suitable transformation of the integral is based on the explicit extraction of the integrand's asymptotics for both $\alpha \to 0$ and $\alpha \to \infty$:

$$\begin{aligned} I_2 = \frac{2i}{|\eta|}\int_{-\infty}^{\infty}\Bigg[&\left(\frac{1}{\alpha+\nu}-\frac{1}{\alpha}\right)|\alpha|e^{i\alpha\xi}\left(K_1(\lambda|\alpha\eta|)-\frac{1}{\lambda|\alpha\eta|}\right)+ \\ &+\left(\frac{1}{\alpha+\nu}-\frac{1}{\alpha}\right)\frac{e^{i\alpha\xi}}{\lambda|\eta|}+\mathrm{sign}(\alpha)e^{i\alpha\xi}K_1(\lambda|\alpha\eta|)\Bigg]d\alpha = I_2^1 + I_2^2 + I_2^3\,. \end{aligned} \tag{24}$$

The first integral can be reduced to the semi-infinite interval $(0,\infty)$, in the following way:

$$\begin{aligned} I_2^1 &= \frac{2i}{|\eta|}\int_{-\infty}^{\infty}\left(\frac{1}{\alpha+\nu}-\frac{1}{\alpha}\right)|\alpha|e^{i\alpha\xi}\left[K_1(\lambda|\alpha\eta|)-\frac{1}{\lambda|\alpha\eta|}\right]d\alpha = \\ &= \frac{2i}{|\eta|}\int_{0}^{\infty}\left(\frac{e^{i\alpha\xi}}{\alpha+\nu}-\frac{e^{i\alpha\xi}}{\alpha}+\frac{e^{-i\alpha\xi}}{\nu-\alpha}+\frac{e^{-i\alpha\xi}}{\alpha}\right)\left[\alpha K_1(\lambda\alpha|\eta|)-\frac{1}{\lambda|\eta|}\right]d\alpha = \\ &= \frac{4i\nu}{\lambda}\int_{0}^{\infty}\frac{\alpha\cos(\alpha\xi)-i\nu\sin(\alpha\xi)}{\alpha(\nu^2-\alpha^2)}\left[\frac{\lambda\alpha K_1(\lambda\alpha|\eta|)}{|\eta|}-\frac{1}{\eta^2}\right]d\alpha \\ &= \frac{4i\nu}{\lambda}\int_{0}^{\infty}\frac{\alpha\cos(\alpha\xi)-i\nu\sin(\alpha\xi)}{\alpha(\nu^2-\alpha^2)}\left[\frac{\lambda\alpha K_1(\lambda\alpha|\eta|)}{|\eta|}-\frac{1}{\eta^2}\right]d\alpha, \end{aligned} \tag{25a}$$

where the Cauchy-type singular integral is, see [28]:

$$\int_0^{\infty} = \lim_{\varepsilon\to+0}\left(\int_0^{\nu-\varepsilon}+\int_{\nu+\varepsilon}^{\infty}\right). \tag{25b}$$

The integrals in (25b) both are absolutely convergent, since the integrand decreases as $O(1/\alpha^2)$ with $\alpha\to\infty$, and its behavior is $O\Big(\alpha|\eta|\ln(\lambda\alpha|\eta|)\Big)$ with $\alpha\to 0$, due to the asymptotics of the Macdonald function for small α [27]. As a result, the quantity I_2^1 becomes a regular function for all values $|\xi,\eta|<\infty$. This means that with any discretization this function may be considered as a usual continuous function.

The quantities I_2^2 and I_2^3 can be expressed in an explicit form, by using some tabulated integrals [26]:

$$\begin{aligned} I_2^2 &= \frac{2i}{\lambda\eta^2}\int_{-\infty}^{\infty}\left(\frac{e^{i\alpha\xi}}{\alpha+\nu}-\frac{e^{i\alpha\xi}}{\alpha}\right)d\alpha = \frac{2}{\lambda\eta^2}\int_{-\infty}^{\infty}\left\{\frac{\sin(\alpha\xi)}{\alpha}-e^{-i\nu\xi}\frac{\sin[(\alpha+\nu)\xi]}{\alpha+\nu}\right\}d\alpha \\ &= \frac{2}{\lambda\eta^2}\left[\pi\,\mathrm{sign}(\xi)-\pi e^{-i\nu\xi}\mathrm{sign}(\xi)\right] = \frac{2\pi\,\mathrm{sign}(\xi)}{\lambda\eta^2}\left(1-e^{-i\nu\xi}\right), \end{aligned} \tag{26}$$

and

$$\begin{aligned} I_2^3 &= \frac{2i}{|\eta|}\int_{-\infty}^{\infty}\mathrm{sign}(\alpha)e^{i\alpha\xi}K_1(\lambda|\alpha\eta|)d\alpha = -\frac{4}{|\eta|}\int_0^{\infty}\sin(\alpha\xi)K_1(\lambda\alpha|\eta|)d\alpha = \\ &= -\frac{4}{|\eta|}\,\frac{\pi\xi}{2\lambda|\eta|\sqrt{\xi^2+(\lambda\eta)^2}} = -\frac{2\pi\xi}{\lambda\eta^2\sqrt{\xi^2+(\lambda\eta)^2}}\,. \end{aligned} \tag{27}$$

4 Numerical Implementation

The numerical algorithm to solve the basic dual integral equation (19) is based upon a discretization, by introducing a two-dimensional discrete mesh. The discrete scheme

should take into account the analytical properties of Eq. (19). The present authors do not know any published work with a thorough investigation of the functional properties of the basic dual integral equation (19). However, some qualitative properties of its kernel are evident. As follows from Eq. (22), by using the asymptotic behavior of the Macdonald function for small argument: $K_1(\zeta) = O(1/\zeta)$, $\zeta \to +0$, as well as from Eqs. (26),(27), the kernel in Eq. (19) is hyper-singular along the wing-span, i.e. over variable y: $O[1/(\eta - y)^2]$, $\eta \to y$. According to the general theory [29,30], if the solution of the one-dimensional hyper-singular integral equation is bounded on the interval $[-1, 1]$, then this solution is unique and automatically vanishes at the side edges $y = \pm 1$. Moreover, within the so-called Method of Discrete Vortices (MDV) [10], it is proved that a simplest quadrature formula may be applied over variable η, to construct an appropriate discrete numerical scheme. For this purpose, one may divide the whole interval $[-1, 1]$ to N_y equal small sub-intervals of length $h_y = 2/N_y$ and to choose a set of nodes taken, to be more specific, at the central points of each sub-interval: $\eta_k = y_k = -1 + (k - 1/2)h_y$, $k = 1, .., N_y$.

Regarding the regular part of the kernel I_2^1, the simple integration along y-axis can be performed in discrete form as the sum of the integrals over small sub-intervals $(y_k - h_y/2, y_k + h_y/2)$. Application of this idea, with $y = y_m$ $(m = 1, .., N_y)$, leads to

$$\begin{aligned} \int_{-1}^{1} I_2^1 \, \gamma(\xi, \eta) d\eta = \frac{4i\nu}{\lambda} \sum_{k=1}^{N_y} \int_{y_k - h_y/2}^{y_k + h_y/2} \left\{ \int_0^\infty G(\alpha, \lambda, \eta - y_m) g(\alpha, \nu, \xi - x) d\alpha \right\} \times \\ \times \gamma(\xi, \eta) d\eta = \frac{4i\nu}{\lambda} \sum_{k=1}^{N_y} h_y \gamma(\xi, y_k) \int_0^\infty G(\alpha, \lambda, y_k - y_m) g(\alpha, \nu, \xi - x) d\alpha, \end{aligned} \tag{28}$$

where the two new functions have been introduced, as follows:

$$\begin{aligned} G(\alpha, \lambda, \eta - y) &= \frac{\lambda\alpha K_1(\lambda\alpha|\eta - y|)}{|\eta - y|} - \frac{1}{(\eta - y)^2}, \\ g(\alpha, \nu, \xi - x) &= \frac{\cos[\alpha(\xi - x)]}{\nu^2 - \alpha^2} - i \frac{\nu \sin[\alpha(\xi - x)]}{\alpha(\nu^2 - \alpha^2)}. \end{aligned} \tag{29}$$

The integration of the continues integrand in Eq. (28) over variable α on the semi-infinite interval is attained numerically in a simple way. As mentioned above, the integrand decreases as $O(1/\alpha^2)$ at $\alpha \to \infty$. Thus, the computation can efficiently be performed by splitting this integral to the two ones:

$$\int_0^\infty G(\alpha, \lambda, y_k - y_m) g(\alpha, \nu, \xi - x) d\alpha = \left(\int_0^{\nu - \varepsilon} + \int_{\nu + \varepsilon}^{B} \right) G(\alpha, \lambda, y_k - y_m) g(\alpha, \nu, \xi - x) d\alpha, \tag{30}$$

where parameter B should be taken sufficiently large, and parameter ε – sufficiently small, as follows from Eq. (25b).

It is proved in [10] that, in the discrete form, the integration of the hyper-singular kernels may be performed just in the same way like for continuous functions. This implies for $y = y_m$:

$$\int_{-1}^{1} I_2^2 \gamma(\xi,\eta)d\eta = \frac{2\pi\left[1-e^{-i\nu(\xi-x)}\right]\mathrm{sign}(\xi-x)}{\lambda}\sum_{k=1}^{N_y}\gamma(\xi,y_k)\int_{y_k-h_y/2}^{y_k+h_y/2}\frac{d\eta}{(\eta-y_m)^2} = \\ = \frac{2\pi\ \left[1-e^{-i\nu(\xi-x)}\right]\mathrm{sign}(\xi-x)}{\lambda}\sum_{k=1}^{N_y}\frac{h_y\gamma(\xi,y_k)}{(y_k-y_m)^2-(h_y/2)^2}\,, \tag{31}$$

while the discretization of the hyper-singular kernel I_2^3 implies, with the use of a certain tabulated integral:

$$\int_{-1}^{1} I_2^3 \gamma(\xi,\eta)d\eta = -\frac{2\pi(\xi-x)}{\lambda}\sum_{k=1}^{N_y}\gamma(\xi,y_k)\int_{y_k-h_y/2}^{y_k+h_y/2}\frac{1}{\sqrt{(\xi-x)^2+\lambda^2(\eta-y_m)^2}}\times \\ \times\frac{d\eta}{(\eta-y_m)^2} = \frac{2\pi}{\lambda}\sum_{k=1}^{N_y}\gamma(\xi,y_k)\left[\frac{\sqrt{(\xi-x)^2+\lambda^2(y_k+h_y/2-y_m)^2}}{(\xi-x)(y_k+h_y/2-y_m)}-\right. \\ \left.-\frac{\sqrt{(\xi-x)^2+\lambda^2(y_k-h_y/2-y_m)^2}}{(\xi-x)(y_k-h_y/2-y_m)}\right]. \tag{32}$$

The discretization of the remaining integral I_1 (4) in the kernel over variable η can be treated as a usual hyper-singular integral, by analogy to I_2^2 and I_2^3. For this aim let us extract explicitly its hyper-singular behavior. The rest is again a continuous

function and can be calculated by analogy to I_2^1, as follows ($y = y_m$):

$$-\frac{\pi e^{-i\nu(\xi-x)}}{\lambda}\int_{-1}^{1} I_1\gamma(\xi,\eta)d\eta = -\frac{\pi e^{-i\nu(\xi-x)}}{\lambda}\int_{-1}^{1}\left[-2\frac{\lambda\nu}{|\eta-y_m|}K_1(\lambda\nu|\eta-y_m|)\right]$$
$$\times\gamma(\xi,\eta)d\eta = \frac{2\pi e^{-i\nu(\xi-x)}}{\lambda}\int_{-1}^{1}\left\{\left[\frac{\lambda\nu K_1(\lambda\nu|\eta-y_m|)}{|\eta-y_m|}-\frac{1}{(\eta-y_m)^2}\right]+\right.$$
$$\left.+\frac{1}{(\eta-y_m)^2}\right\}\gamma(\xi,\eta)d\eta = \frac{2\pi e^{-i\nu(\xi-x)}}{\lambda}\times \tag{33}$$
$$\times\sum_{k=1}^{N_y}\gamma(\xi,y_k)\int_{y_k-h_y/2}^{y_k+h_y/2}\left[G(\nu,\lambda,\eta-y_m)+\frac{1}{(\eta-y_m)^2}\right]d\eta = \frac{2\pi e^{-i\nu(\xi-x)}}{\lambda}\times$$
$$\times\sum_{k=1}^{N_y}\gamma(\xi,y_k)\left[h_y\,G(\nu,\lambda,y_k-y_m)+\frac{h_y}{(y_k-y_m)^2-(h_y/2)^2}\right],$$

since function G is continuous.

It should be noted that expressions (32) and (33) in the aggregate correspond to the standard discretization in the classical theory of lifting surface in a stationary flow ($\nu = 0$), in frames of the MDV [10].

Now let us pass to the numerical treatment along the chord direction, i.e. along axis x. The MDV prescribes [10] that the following mesh structure may be arranged, to provide stable calculations, by introducing the two different grids – separately for the internal variable ξ and the external one x. With this treatment, the nodes of the former are placed in the middle between respective nodes of the latter: $\xi_j = -1 + jh_x,\ \ x_n = \xi_n + h_x/2,\ \ (n, j = 1, ..N_x)$, $h_x = 2/(N_x+1)$. Here N_x is the dimension of the grid along the chord direction x. It is proved in [10] that such a grid guarantees the automatical validity of the Kutta-Joukowski hypothesis of bounded aerodynamic pressure just on the edge closest to a node of the external grid. Since in our case $x_1 = -1 + 3h_x/2$, but $x_{N_x} = -1 + (N_x + 1/2)h_x = 1 - h_x/2$, hence the trailing edge $x = 1$ is the closest one to the node x_{N_x}. Therefore, the applied discretization grids provide the Kutta-Joukowski condition on the true trailing edge $x = 1$. Within this method, the quadrature formula for the Cauchy-type integral over variable ξ is simply a summation over grid nodes $\xi = \xi_j$, $(j = 1, ..N_x)$, then multiplying this sum by the grid step h_x.

The performed discretization leads to the following representation of the left-hand

side in Eq. (19)–(21):

$$\frac{h_x c}{2\pi\lambda\rho u_0^2}\sum_{j=1}^{N_x}\sum_{k=1}^{N_y}\gamma(\xi_j,y_k)\left[\frac{2i\nu h_y}{\pi}\int_0^\infty G(\alpha,\lambda,y_k-y_m)g(\alpha,\nu,\xi_j-x_n)d\alpha+\right.$$

$$+h_y e^{-i\nu(\xi_j-x_n)}G(\nu,\lambda,y_k-y_m)+h_y\frac{e^{-i\nu(\xi_j-x_n)}[1-\mathrm{sign}(\xi_j-x_n)]+\mathrm{sign}(\xi_j-x_n)}{(y_k-y_m)^2-(h_y/2)^2} \qquad (34)$$

$$\left.+\frac{\sqrt{(\xi_j-x_n)^2+\lambda^2(y_k+h_y/2-y_m)^2}}{(\xi_j-x_n)(y_k+h_y/2-y_m)}-\frac{\sqrt{(\xi_j-x_n)^2+\lambda^2(y_k-h_y/2-y_m)^2}}{(\xi_j-x_n)(y_k-h_y/2-y_m)}\right].$$

Let us rewrite our problem in the following matrix form

$$A\gamma = u\,. \qquad (35)$$

It should be noted that, when arranging the dicretization, index j is related to the internal variable along axis x, index n – to the external variable along the same axis, index k is coupled with the internal variable along axis y, and index m – with the external variable along the same axis. The structure of the matrix A is such that each its block $A^{m,k}$ corresponds to a chosen pair of nodes m,k on y-axis ($m,k=1,..,N_y$), and the elements of this block are values of the kernel taken for nodes n,j on x-axis ($n,j=1,..,N_x$). The vector $\gamma=\gamma(\xi_j,y_k)$ also has a block structure, where each block k contains the values of the unknown function γ at the nodes ξ_j of the corresponding y_k-band. Mathematically, this is expressed in the following indexing $\gamma(\xi_j,y_k)=\gamma_{j+(k-1)N_x}$, where $j=1,..,N_x$ and $k=1,..,N_y$. The right-hand side vector $u=(i\nu W-\partial W/\partial x)(x_n,y_m)$ is written similarly. The indices of this vector have the form $u(x_n,y_m)=u_{n+(m-1)N_x}$ with $n=1,..,N_x$ and $m=1,..,N_y$.

In other words, the matrix element $a_{n,j}^{m,k}$ is located at the intersection of the row number $n+(m-1)N_x$ and the column number $j+(k-1)N_x$. Let us note, that upper indices in the matrix designate the number of a block and the lower ones – the position of the element in this block. Herewith, inside each block one moves along x-axis, while the change of the block itself changes location on the grid along variable y.

Since the dimension of the unknown vector γ in Eq. (35) is $N_x\cdot N_y$ (this means N_y blocks with N_x elements in each of them), the total number of elements in matrix A is $(N_x\cdot N_y)^2$ and obviously, the matrix is fully populated.

However, substituting quantities ξ,x,y in their discrete form to Eq. (16), one can see that the kernel depends only on the difference of indices, namely:

$$y_k-y_m=(k-m)h_y,\quad \xi_j-x_n=(j-n)h_x-h_x/2 \qquad (36)$$

As a result, the number of distinct elements of the matrix A is significantly reduced, because in each block there are only $2N_x - 1$ essentially different elements $a_{n,j} = a_{j-n}$. Moreover, the blocks of the matrix are also repeated $A^{m,k} = A^{k-m}$. The properties of such matrices and their advantages are discussed in the next section.

5 Matrix-Vector Multiplication

It is well-known in which way one can reduce the cost of the matrix-vector multiplication in the case when the matrix is sparse. Also, there are some approaches for dense matrices if they have some special structure, in particular for Vandermonde, Cauchy, Toeplitz and Hankel matrices. The matrix of the system (35) also possesses a certain specific structure. Namely, it is Block-Toeplitz with Toeplitz Blocks (BTTB), or two-level Toeplitz matrix. This means that each block $A^{m,k}$ of our matrix is represented by a Toeplitz matrix.

A matrix is called Toeplitz if its elements depend only on the difference of the indices [25], in other words, if $a_{n,j} = a_{n-j}$ Thus, the full information about the matrix coefficients can be collected in the first row and first column of the matrix and it is sufficient to define only one vector of length $2N_x - 1$ in the memory storage for the matrix of dimension $N_x \cdot N_x$ [31–34]. In the BTTB case the Toeplitz structure spreads out into blocks of the matrix. In our case there is also a symmetry in a block distribution, hence $A^{m,k} = A^{|m-k|}$, or in the matrix representation

$$A = \begin{pmatrix} A^0 & A^1 & \dots & A^{N_y-2} & A^{N_y-1} \\ A^1 & A^0 & A^1 & & A^{N_y-2} \\ \vdots & A^1 & A^0 & \ddots & \vdots \\ A^{N_y-2} & & \ddots & \ddots & A^1 \\ A^{N_y-1} & A^{N_y-2} & \dots & A^1 & A^0 \end{pmatrix}. \tag{37}$$

where each block $A^{m,k}$ is represented by the non-symmetric Toeplitz matrix

$$A^{m,k} = \begin{pmatrix} a_0^{m,k} & a_{-1}^{m,k} & \dots & a_{-(N_x-2)}^{m,k} & a_{-(N_x-1)}^{m,k} \\ a_1^{m,k} & a_0^{m,k} & a_{-1}^{m,k} & & a_{-(N_x-2)}^{m,k} \\ \vdots & a_1^{m,k} & a_0^{m,k} & \ddots & \vdots \\ a_{N_x-2}^{m,k} & & \ddots & \ddots & a_{-1}^{m,k} \\ a_{N_x-1}^{m,k} & a_{N_x-2}^{m,k} & \dots & a_1^{m,k} & a_0^{m,k} \end{pmatrix}. \tag{38}$$

It is clear, that, by knowing the structure of the matrix A, we need to collect only the first row and the first column of it to storage all matrix just in one vector of length $2N_xN_y - 1$. This is a big advantage for the matrix with dense structure and it provides a good basis, to construct a fast matrix-vector multiplication algorithm [32–34].

In the case of one-level Toeplitz matrices this algorithm is based on the convolution theorem and the application of the Fast Fourier Transform (FFT) [22, 24, 25]. This theorem can be expressed in the matrix form: $C\lambda = w$, where λ is an arbitrary known vector of length N_x, vector w is the resulting unknown right-hand side, matrix C is a periodic Toeplitz matrix with elements

$$C = \begin{pmatrix} c_0 & c_{N_x-1} & \cdots & c_2 & c_1 \\ c_1 & c_0 & c_{N_x-1} & & c_2 \\ \vdots & c_1 & c_0 & \ddots & \vdots \\ c_{N_x-2} & & \ddots & \ddots & c_{N_x-1} \\ c_{N_x-1} & c_{N_x-2} & \cdots & c_1 & c_0 \end{pmatrix}. \tag{39}$$

which is often called a circulant matrix. The singular value decomposition of such a matrix is well known and can be represented as $C = F^{-1}\Lambda F$, where the Fourier matrix F is a special type of the Vandermonde matrix with the elements $F_{nm} = e^{2\pi inm/N}$, and matrix Λ is a diagonal matrix with singular values of C on its diagonal, which can be obtained by multiplying the Fourier matrix by the first row of C. Thus, the multiplication of the matrix C by a vector can be done by applying the FFT method three times with the computational cost $3 \cdot N \log_2(N)$, since each FFT can be performed with $N \log_2(N)$ operations.

In order to apply this algorithm to a Toeplitz matrix, one can extend the Toeplitz matrix to a matrix of a larger size but with circulant property [23]

$$\begin{pmatrix} S & \boxtimes \\ \boxtimes & S \end{pmatrix} \begin{pmatrix} \lambda \\ 0 \end{pmatrix} = \begin{pmatrix} S\lambda \\ \boxtimes\lambda \end{pmatrix} \tag{40}$$

Such extension can be done for any one-level Toeplitz matrix S. However, in the two-level case this approach should be applied on each level [20]. Application of this

technique on the block level can be expressed as the following matrix $\widetilde{A} =$

$$\left(\begin{array}{ccccc|ccccc}
\widetilde{A}^0 & \widetilde{A}^1 & \dots & \widetilde{A}^{N_y-2} & \widetilde{A}^{N_y-1} & 0 & \widetilde{A}^{N_y-1} & \dots & \widetilde{A}^2 & \widetilde{A}^1 \\
\widetilde{A}^1 & \widetilde{A}^0 & \widetilde{A}^1 & & \widetilde{A}^{N_y-2} & \widetilde{A}^{N_y-1} & 0 & \widetilde{A}^{N_y-1} & & \widetilde{A}^2 \\
\vdots & \widetilde{A}^1 & \widetilde{A}^0 & \ddots & \vdots & \vdots & \widetilde{A}^{N_y-1} & 0 & \ddots & \vdots \\
\widetilde{A}^{N_y-2} & & \ddots & \ddots & A^1 & \widetilde{A}^2 & & \ddots & \ddots & \widetilde{A}^{N_y-1} \\
\widetilde{A}^{N_y-1} & \widetilde{A}^{N_y-2} & \dots & \widetilde{A}^1 & \widetilde{A}^0 & \widetilde{A}^1 & \widetilde{A}^2 & \dots & \widetilde{A}^{N_y-1} & 0 \\
\hline
0 & \widetilde{A}^{N_y-1} & \dots & \widetilde{A}^2 & \widetilde{A}^1 & \widetilde{A}^0 & \widetilde{A}^1 & \dots & \widetilde{A}^{N_y-2} & \widetilde{A}^{N_y-1} \\
\widetilde{A}^{N_y-1} & 0 & \widetilde{A}^{N_y-1} & & \widetilde{A}^2 & \widetilde{A}^1 & \widetilde{A}^0 & \widetilde{A}^1 & & \widetilde{A}^{N_y-2} \\
\vdots & \widetilde{A}^{N_y-1} & 0 & \ddots & \vdots & \vdots & \widetilde{A}^1 & \widetilde{A}^0 & \ddots & \vdots \\
\widetilde{A}^2 & & \ddots & \ddots & \widetilde{A}^{N_y-1} & \widetilde{A}^{N_y-2} & & \ddots & \ddots & \widetilde{A}^1 \\
\widetilde{A}^1 & \widetilde{A}^2 & \dots & \widetilde{A}^{N_y-1} & 0 & \widetilde{A}^{N_y-1} & \widetilde{A}^{N_y-2} & \dots & \widetilde{A}^1 & \widetilde{A}^0
\end{array}\right) \tag{41}$$

where each block $\widetilde{A}^{|m-k|}$ is an extension of $A^{|m-k|}$ to a circulant matrix, like in (26). Here, to be more specific, we assume that $N_x = N_y = 2^M$. Similarly to the BTTB, the matrix of the type (41) is called Block-Circulant with Circulant Blocks (BCCB) or two-level circulant matrix [20]. It is easily seen that in our case its dimension is $(4N_xN_y)^2$. Like the one-level circulant matrix, the singular value decomposition of the BCCB can be performed by the application of the two-dimensional FFT algorithm. The matrix-vector multiplication and the solution of the SLAE with the matrix (41) cost together $O(6 \cdot 4N_xN_y \log_2(4N_xN_y))$ arithmetic operations.

However, to perform fast matrix-vector multiplication algorithm we also need to extend our vector for an appropriate form [20]. For a vector z of dimension N_xN_y this extension can also be done in the two-level way:

$$e^T = \left(\underbrace{z^1 \;\; 0 \;\; z^2 \;\; 0 \;\; \dots \;\; z^{N_y-1} \;\; 0 \;\; \overbrace{z^{N_y} \;\; 0}^{2N_x \text{ elements}}}_{2N_xN_y \text{ elements}} \;\Big|\; \underbrace{0 \;\; 0 \;\; \dots \;\; 0 \;\; 0}_{2N_xN_y \text{ elements}} \right), \tag{42}$$

where the superscript T denotes the transpose operation and the superscript above the initial vector z means its block. After the multiplication is performed, some additional work should be done to collect proper information from the vector of dimension $4N_xN_y$ in a vector of dimension N_xN_y. Firstly, we "cut the tail" and keep only the first part of the obtained array, for $j \le 2N_xN_y$, by taking only first N_y blocks ($n \le N_y$). In the same way we collect only first part of each block by restricting index $j \le N_x$. In other words, after the multiplication $\widetilde{A}e = \widetilde{s}$, we take only $s_j^n = \widetilde{s}_j^n$, $j = 1, 2, \dots, N_x$, $n = 1, 2, \dots, N_y$.

It is easy to estimate that the application of the described ideas inside the BiCG algorithm reduces the total computational cost to $N_{it} \cdot 48 N_x N_y \log_2(4 N_x N_y)$.

6 Preconditioning Technique

As shown in the next section, the application of the BiCG algorithm efficiently solves the linear system (35), but the number of iterations significantly depends on the size of the numerical grid. This behavior is connected with the condition number of the matrix A and with the distribution of its eigenvalues. To improve these parameters, one may apply the preconditioning technique [22, 23]. It means, that instead of solving the initial SLAE, one can more efficiently solve the modified system

$$P^{-1} A \gamma = P^{-1} u, \tag{43}$$

where P is a preconditioner matrix, which reduces the condition number of the matrix $P^{-1}A$ and aggregates its eigenvalues around 1. With this treatment, the number of iterations of the BiCG method can be significantly reduced. The preconditioned BiCG method [35,36] can be rewritten in the following form:

$$\begin{gathered}
\alpha_i = (\hat{r}_{i-1}, P^{-1} r_{i-1}) / (\hat{z}_i, A z_i), \\
\gamma_i = \gamma_{i-1} + \alpha_i z_i, \\
r_i = r_{i-1} - \alpha_i A z_i, \\
\hat{r}_i = \hat{r}_{i-1} - \alpha_i A^T \hat{z}_i, \\
\beta_i = (\hat{r}_i, P^{-1} r_i) / (\hat{r}_{i-1}, P^{-1} r_{i-1}), \\
z_{i+1} = P^{-1} r_i + \beta_i z_i \\
\hat{z}_{i+1} = (P^T)^{-1} \hat{r}_i + \beta_i \hat{z}_i.
\end{gathered} \tag{44}$$

It is assumed that the inverse to the preconditioner matrix can be easily constructed, this means that the system $P w_i = r_i$ can be solved efficiently. In the case of one-level Toeplitz matrices the construction of the preconditioner matrix is done by using the circulant preconditioner [37-42], because, as discussed in the previous section, the solution to the SLAE with such a matrix can be constructed by applying the rapid FFT scheme. The same idea can be applied in the two-level case, where BCCB should be taken as the preconditioner matrix.

The generalization of the T. Chan optimal circulant preconditioner in the two-level case can be easily constructed from the elements of the initial matrix [20,21]. Its first

row vector is as follows:

$$c_{i,1}^{j,1} = \begin{cases} a_{1,1}^{1,1}, & i = j = 1 \\ \dfrac{(N_y - (j-1))a_{1,1}^{1,j} + (j-1)a_{1,1}^{N_y-(j-2),1}}{N_y} & i = 1, j > 1 \\ \dfrac{(N_x - (i-1))a_{1,i}^{1,1} + (i-1)a_{N_x-(i-2),1}^{1,1}}{N_y} & i > 1, j = 1 \\ \bar{c}_{i,1}^{j,1}/(N_x N_y) & i > 1, j > 1 \end{cases} \tag{45}$$

where

$$\begin{aligned} \bar{c}_{i,1}^{j,1} = (N_y - (j-1))(N_x - (i-1))a_{1,i}^{1,j} + (j-1)(N_x - (i-1))a_{1,i}^{N_y-(j-2),1} \\ +(N_y - (j-1))(i-1)a_{N_x-(i-2),1}^{1,j} + (j-1)(i-1)a_{N_x-(i-2),1}^{N_y-(j-2),1}, \end{aligned} \tag{46}$$

and, as before, the superscripts refer to the block number and subscripts – to the elements inside this block. It is easy to calculate, that total number of operations for such an algorithm is $N_{it} \cdot N(6\log_2(N) + 48\log_2(4N))$.

A more advanced fast method to solve SLAEs with the two-level Toeplitz matrix can be found in [3]. The method is based on the construction of the inverse matrix via iterative Newton-Hotelling-Schulze's method with the use of the wavelet transforms and the low-rank tensor approximations. However, from the physical point of view, the authors in the discussed paper do not take into account the Kutta-Joukowski hypothesis. The kernel of the integral equation is a characteristic hyper-singular kernel. As a result, in the case of the rectangular grid [3], the matrix T of the SLAE is of doubly-symmetrical form and all its eigenvalues are real, this allows the authors to solve it by using the simple CG algorithm. For example, there are required only 39 iterations of the CG method without preconditioning to achieve the accuracy 10^{-11} on the rectangular grid $N = N_x \cdot N_y = 1024$, and only 15 iterations with the usage of the optimal T. Chan preconditioner (45)-(46).

It can easily be seen that the eigenvalues of our matrix A from the system (35) are complex-valued, but the multiplication of the matrix A by the T. Chan two-level circulant preconditioner aggregate the most part of the eigenvalues of the resulting matrix around the real value 1. This fact decreases essentially the number of iterations in the BiPCG method.

Another efficient version from the family of CG methods is the Conjugate Gradient Squared method (CGS), which preconditioned version can be written out as follows

[35]:

$$\begin{aligned}
\alpha_n &= (\tilde{r}, r_{n-1})/(\tilde{r}, AC^{-1}z_n),\\
g_n &= r_{n-1} + (\tilde{r}, r_{n-1})q_{n-1},\\
q_n &= g_n - \alpha_n AC^{-1}z_n,\\
\gamma_n &= \gamma_{n-1} + \alpha_n C^{-1}(g_n + q_n),\\
r_n &= r_{n-1} - \alpha_n AC^{-1}(g_n + q_n),\\
\beta_n &= (\tilde{r}, r_n)/(\tilde{r}, r_{n-1}),\\
z_{n+1} &= g_n + \beta_n(q_n + \beta_n z_n)
\end{aligned} \tag{47}$$

One can derive from this algorithm a CGS method without preconditioning by simply putting matrix C to be the unit matrix. Also, this method does not involve the transpose of the initial matrix, which can be a good advantage in some cases.

7 Numerical Experiments

We have performed many tests by using the discussed methods applied to Eq. (19). First, we test three different iterative methods such as CGNE, BiCG and CGS. As shown in the numerical examples, in the case when the number of nodes $N_x = N_y = 2^6$, i.e. the overall size of the matrix is $N = 2^{12}$, the CGNE and CGS methods diverge, while the BiCG solves the problem in 165 iterations with the accuracy 10^{-10}. When the T. Chan BCCB preconditioner is used, only 42 steps are needed to attain the same accuracy.

For the first method, namely the CGNE, it is clear that the condition number of the matrix $A^T A$ is too large and certainly, this is the main reason of the divergency of the method. Regarding the CGS method, it is well known that, being faster than the BiCG, it is not so stable as the latter. Specifically, for the numerical experiment under consideration, the CGS method without preconditioner can only give the accuracy 10^{-7} for $N_x = N_y = 2^6$. For this reason we recommend to use the BiCG method in the problem under discussion.

In the table 1 the speed of the different modifications of the BiCG approach is reflected in comparison with the Gauss elimination method. The "fast BiCG" refers to the BiCG with the fast matrix-vector multiplication for the BTTB matrix and the "fast BiPCG" - to the preconditioned method with both the fast matrix-vector multiplication and the T. Chan two-level circulant preconditioner. In our calculations, similarly to [1], we take the following parameters: $c = 0.1\,m$, $\ell = 0.5\,m$, $u_0 = 10\,m/s$,

$\rho = 1.225\, kg/m^3$.

Once the values of the dimensional quantities c and u_0 are chosen, the value of the dimensionless Strouhal number $\nu = \omega c/u_0$ is defined only by the circular frequency $\omega = 2\pi f$, where f is a cyclic frequency measured in Hertz. Since under natural physical conditions the cyclic frequency f is unlikely greater than $15\, Hz$, then with the accepted physical parameters the Strouhal number ν is certainly less than 1. That is why all examples below with the demonstrated numerical results are presented for $0 < \nu < 1$.

For each of these methods it is indicated the overall number of arithmetic operations, needed to evaluate the corresponding algorithm. It is notable, that one iteration of the fast BiPCG is more expensive than one iteration of the fast BiCG, since the former involves $6N\log_2(N)$ additional operations, needed to construct the fast solution of the convolution system. However, due to the application of the preconditioning technique, the total number of iterations in the fast BiPCG is much smaller than in the fast BiCG. As a result, the overall cost of the fast BiPCG is at least twice cheaper than its non-preconditioned version.

For the last two algorithms the number of iterations needed to attain the desired accuracy is also presented. It is clear that the classical BiCG algorithm needs the same amount of iterations as the fast BiCG, for this reason the corresponding row is omitted in the table 1.

From the computational point of view, not only the total number of operations is critical. Another important parameter is the memory allocated to collect the data involved in the algorithm. In our case the more expensive data in this sense is the matrix storage. It is clear that for both the Gauss elimination technique and the classical BiCG method (first two rows in the table 1) one needs to collect the matrix with N^2 non-zero elements. However, for the "fast" versions of BiCG, presented in the last two rows of the table 1, only the allocation of vectors with the maximum size $4N\log_2(4N)$ is needed. In particular, this explains why both the Gauss and the classical BiCG cannot solve the system larger than with $N^2 = (16384 \times 16384)$ elements in the used PC.

The comparison of the two "fast" algorithms shows that in practice, the difference between these two methods is insignificant. However, for extremely high number of nodes $N = 4^9$ only the fast BiPCG can solve the problem.

Table 1. Dependence of the execution time upon total number of nodes N (s = sec), with an Intel Core i7-3770 four-cores CPU and 4 GB of DDR3 SDRAM

Method	number of nodes $N = N_x \cdot N_y = 4^M$					
	M=4	M=5	M=6	M=7	M=8	M=9
	256	1024	4096	16384	65536	262144
Gauss	**0.013 s**	**1.615 s**	**158.1 s**	**-**	**-**	**-**
N^3	$1.7 \cdot 10^7$	$1.1 \cdot 10^9$	$6.9 \cdot 10^{10}$	$4.4 \cdot 10^{12}$	$2.8 \cdot 10^{14}$	$1.8 \cdot 10^{16}$
BiCG	**0.014 s**	**1.125 s**	**32.63 s**	**-**	**-**	**-**
$N_{it} \cdot 2 \cdot N^2$	$6.3 \cdot 10^6$	$1.4 \cdot 10^8$	$3.1 \cdot 10^9$	$7.8 \cdot 10^{10}$	$2.1 \cdot 10^{12}$	-
fast BiCG	**0.024 s**	**0.189 s**	**0.828 s**	**3.69 s**	**35.08 s**	**-**
$N_{it} \cdot 48N \log_2(4N)$	$5.9 \cdot 10^6$	$3.8 \cdot 10^7$	$2.6 \cdot 10^8$	$1.8 \cdot 10^9$	$1.4 \cdot 10^10$	-
N_{it}	*48*	*65*	*93*	*145*	*242*	-
fast BiPCG	**0.015 s**	**0.115 s**	**0.516 s**	**1.67 s**	**11.43 s**	**59.78 s**
$N_{it} \cdot 54N \log_2(4N)$	$2.9 \cdot 10^6$	$1.8 \cdot 10^7$	$1.1 \cdot 10^8$	$6.5 \cdot 10^8$	$3.9 \cdot 10^9$	$2.2 \cdot 10^{10}$
N_{it}	*21*	*27*	*35*	*46*	*62*	*77*

Finally, Figs. 2–6 show the calculated solution vector $|\gamma|$ in some cross-sections of the wing, in the case $W(x, y) \equiv 1$. It is notable that the qualitative behavior of the solution in our problem is absolutely different from the calculations presented in [3], where the resultant vector is symmetric. It is easily seen that with higher number of nodes it is possible to calculate large values of the unknown vector near the edge $x = -1$ more accurately. It should also be noted that the magnitude of the solution grows with the increasing parameter ν.

Analogous solution in the case, when wing's surface is a periodic function along the span, is demonstrated in Fig. 7.

8 Conclusions

1. The integral equation of the oscillating wing is adopted for application of various fast numerical schemes. The kernel of the basic dual integral equation possesses a hyper-singular behavior along the wing span, variable y, and a Cauchy-type singular behavior along the chord, variable x. In the case $\nu = 0$ the equation corresponds to the classical theory of wing in the stationary stream (the lifting surface theory) [18].

2. In the discrete form the basic equation is reduced to a SLAE with a specific Block-Toeplitz matrix structure. Various non-stationary iterative methods are tested

to solve the problem at hand. The Bi-Conjugate Gradient Method demonstrates higher efficiency than other improved versions of the CG method. It is established that among other tested methods, the BiPCG method with the help of the two-dimensional FFT can solve the problem for extremely high number of nodes with an appropriate time and computer memory.

3. For the correct treatment of the basic dual integral equation the Kutta-Joukowski hypothesis should be applied, this means that the solution is bounded at the trailing edge $x = 1$ and unbounded at the leading edge $x = -1$. The qualitative properties of the solution are absolutely different from those in the problem for wing's vibration in the motionless fluid [19]. The solution of the latter is symmetric along both wing-span and chord directions. In contrast to this, the solution of the problem at hand is symmetric along the wing-span direction and, due to the Kutta-Joukowski condition, is strongly asymmetric along the chord direction.

4. The constructed exact numerical method allows us to estimate the precision of the approximate asymptotic solution valid in the case of large aspect ratio $\lambda \gg 1$ [1]. Table 2 demonstrates the comparison between the present direct numerical values of the aerodynamic force acting over the surface of the wing, namely the quantity (17). It is clearly seen from Table 2 that the numerical results approach the asymptotic one with increasing λ, for all values of the Strouhal number on the interval $\nu \in (0, 1)$, $W(x, y) \equiv 1$. Thus, for $\lambda = 10$ the maximum relative error of the asymptotic solution is around 17%, and for $\lambda = 20$ is around 9%.

5. **Let us briefly specify what is new in the present work and what is already available in the literature.**

   • The basic dual integral equation is well known in the two cases: (i) the stationary flow ($u_0 \neq 0$, $\omega = 0$) [10,18], and (ii) the oscillations of the plate placed in a fluid at rest ($u_0 = 0$) harmonic in time ($\omega \neq 0$) [19]. The considered case of the harmonic oscillations of the plate in a uniform flow ($u_0 \neq 0$, $\omega \neq 0$) is less known, and a standard derivation requires a huge amount of mathematical transformations, like in [18]. Here we give a short development by using the double Fourier transform.

   • In those two cases above, (i) and (ii), the kernel of the basic integral equation can be written explicitly in terms of some elementary

functions. In the problem at hand the kernel (20)-(21) is expressed in terms of the dual Fourier transform, which cannot be calculated explicitly. The representation for the kernel in the form (24)–(27) is absolutely new, and the key point there is the extraction of its regular part (25a) as a certain integral, which can be implemented numerically in a simple way, plus two singular kernels of some explicit elementary form. This idea is allied to some classical ideas in the theory of asymptotic expansions (see, for example [30], with further helpful references), which is to retain the singularities of the integrand in (23), for small and large arguments, in a regular part of the kernel, and to extract all singularities of the kernel explicitly.

• Once the disretization of the dual integral equation is performed, the arising matrix is of a Toeplitz-Blocks structure. Since in the case of the dual equation the total size of the grid grows as the second power of the linear grid dimension, then the computer expenses grow as the sixth power of the linear dimension, if one applies any direct numerical implementation like Gauss elimination technique or something similar. Hence, in practice, this equation cannot be numerically resolved with a required precision. The natural idea is then to take into account the specific geometric structure of the matrix under the disretization. The numerical treatment applied in the present paper is based on the preconditioned bi-conjugate gradient method with the two-level T.Chan circulant preconditioner, which is absolutely new when being applied to the problem on plate's harmonic oscillation in the flow.

• Generally, the application of the numerical techniques applied, namely, the BiPCG with a circulant preconditioner, is of course not new. However, the present authors could not find in literature a detailed comparison of various algorithms applied to the matrix of the specific structure arisen. The detailed analysis of application of various iterative methods from the CG-family of algorithms allows us to identify a certain method, which is the best for the considered types of problems, in the sense of both the running time and the random-access memory. This is in fact a combination of the BiPCG method and the fast matrix-vector multiplication on each iteration step performed by the two-level

convolution with the FFT algorithm.

Acknowledgements

The present work has been supported by the Russian Ministry for Education and Science, Project 9.5794.2017/8.9.

The authors express their gratitude to the anonymous reviewer for his/her very helpful critical comments.

Table 2. The amplitude of the aerodynamic force $|P| \cdot 10^{-3}$ versus parameters ν and λ: comparison between the numerical values for different λ and the "asymptotic" value for $\lambda \to \infty$ [1]: $W(x, y) \equiv 1$

ν	0.1	0.2	0.3	0.4	0.5	0.6	0.7	0.8	0.9	1.0
$\lambda = 5$	0.467	0.891	1.294	1.718	2.169	2.652	3.216	3.827	4.503	5.279
$\lambda = 10$	0.552	1.013	1.438	1.861	2.327	2.835	3.419	4.052	4.751	5.538
$\lambda = 20$	0.601	1.077	1.504	1.935	2.401	2.919	3.498	4.143	4.857	5.643
asymp.	0.647	1.128	1.537	1.927	2.333	2.776	3.273	3.833	4.463	5.168

References

[1] M.A. Sumbatyan, A.E. Tarasov, A mathematical model for the propulsive thrust of the thin elastic wing harmonically oscillating in a flow of non-viscous incompressible fluid, *Mechanics Research Communications*, 2015, **68**, 83–88.

[2] K.D. Jones, A collaborative numerical and experimental investigation of flapping-wing propulsion, *AIAA Paper No. 2002-0706*, 2002, 1-14.

[3] J.M. Birch, M.H. Dickinson, Spanwise flow and the attachment of the leadingedge vortex on insect wings *Nature*, 2001, **412**, 729-733.

[4] S.P. Sane, M.H. Dickinson, The control of flight force by a flapping wing: lift and drug production, *J. Experiment. Biol.*, 2001, **204**, 2607-2626.

[5] D.A. Read, F.S. Hover, M.S. Triantafyllou, Forces on oscillating foils for propulsion and maneuvering, *J. Fluids Struct.*, 2003, **17**, 163-183.

[6] R. Ramamurti, W.C. Sandberg, A three-dimensional computational study of the aerodynamic mechanisms of insect flight, *J. Experiment. Biol.*, 2002, **205**, 1507-1518.

[7] A. Leonard, Vortex methods for flow simulation, *J. Comput. Phys.*, 1980, **37**, 289-335.

[8] R.I. Lewis, *Vortex Element Methods for Fluid Dynamic Analysis of Engineering Systems*, Cambridge University Press: Cambridge, 2005.

[9] G. Morgenthal, *Aerodynamic Analysis of Structures Using High-resolution Vortex Particle Methods: PhD thesis*, University of Cambridge. Department of Engineering: Cambridge, 2002.

[10] S.M. Belotserkovsky, I.K. Lifanov, *Method of Discrete Vortices*, CRC Press: Boca Raton, Florida, 1992.

[11] D.A. Peters, M.A. Hsieh, A. Torrero, A state-space airloads theory for flexible airfoils, *J. Amer. Helicopter Soc.*, 2007, **52**, 329-342.

[12] W.P. Walker, M.J. Patil, Unsteady aerodynamics of deformable thin airfoils, *J. Aircraft*, 2014, **51**, 1673-1680.

[13] C.O. Johnston, W.H. Mason, C. Han, Unsteady thin airfoil theory revisited for a general deforming airfoil, *J. Mech. Sci. Tech.*, 2010, **24**, 2451-2460.

[14] D. Mateescu, M. Abdo, Theoretical solutions for unsteady flows past oscillating flexible airfoils using velocity singularities, *J. Aircraft*, 2003, **40**, 153-163.

[15] J.M. Anderson, K. Streitlien, D.S. Barrett, M.S. Triantafyllou, Oscillating foils of high propulsive efficiency, *J. Fluid Mech.*, 1998, **360**, 41-72.

[16] I.H. Tuncer, M. Kaya, Optimization of flapping airfoils for maximum thrust and propulsive efficiency, *AIAA journal*, 2005, **43**, 2329-2336.

[17] U. Gulcat, Propulsive force of a flexible flapping thin airfoil, *J. Aircraft*, 2009, **46**, 465-473.

[18] R.L. Bisplinghoff, H. Ashley, R.L. Halfman, *Aeroelasticity*, Addison-Wesley: Cambridge, 1955.

[19] I.V. Oseledets, E.E. Tyrtyshnikov, Approximate inversion of matrices in the process of solving a hypersingular integral equation, *Computational Mathematics and Mathematical Physics*, 2005, **45**, 302–313.

[20] D.A. Bini, A family of modified regularizing circulant preconditioners for two-levels Toeplitz systems, *Computers and Mathematics with Applications*, 2004, **48**, 755–768.

[21] C. Van der Mee, G. Rodriguez, S. Seatze, Fast computation of two-level citculant preconditiones, *Numerical Algorithms*, 2006, **41**, 275–295.

[22] G. H. Golub, C. F. van Loan, *Matrix Computations* **, Johns Hopkins Univ. Press: Baltimore, Md., 1996.**

[23] E. E. Tyrtyshnikov, *A Brief Introduction to Numerical Analysis***, Springer: New York, 1997.**

[24] C. Van Loan, *Computational Frameworks for the Fast Fourier Transform***, SIAM: Philadelphia, 1992.**

[25] W.H. Press, S.A. Teukolsky, W.T. Vetterling, B.P. Flannery, *Numerical Recipes: The Art of Scientific Computing, 2nd Edition***, Cambridge University Press: Cambridge, 1992.**

[26] A.P. Prudnikov, Y.A. Brychkov, O.I. Marichev, *Integrals and Series, Vol. 1*, Gordon & Breach: Amsterdam, 1986.

[27] M. Abramowitz, I. Stegun. *Handbook of Mathematical Functions*, Dover: New York, 1965.

[28] F.D. Gakhov, *Boundary Value Problems*, Pergamon Press: Oxford, 1966.

[29] S.G. Samko, *Hypersingular Integrals and Their Applications*, CRC Press: Boca Raton, Florida, 2002.

[30] M.A. Sumbatyan, A. Scalia, *Equations of Mathematical Diffraction Theory*, CRC Press: Boca Raton, Florida, 2005.

[31] W. Trench, An algorithm for the inversion of finite Toeplitz matrices,*SIAM Journal on Applied Mathematics***, 1964, 12, 512–522.**

[32] F. de Hoog, A new algorithm for solving Toeplitz systems of equations,*Linear Algebra and its Applications*, **1987, 88/89, 123–138.**

[33] G. Ammar, W. Gragg, Superfast solution of real positive definite Toeplitz systems, *SIAM Journal on Matrix Analysis and Applications*, **1988, 9, 61–76.**

[34] V. V. Voevodin, E. E. Tyrtyshnikov, *Computational Processes with Toeplitz Matrices*, **Nauka: Moscow, 1987.**

[35] *Templates for the Solution of Linear Systems: Building Blocks for Iterative Methods, 2nd Edition*, (edited by R. Barrett, M. Berry), SIAM: Philadelphia, 1994.

[36] R.H-F. Chan, X-Q. Jin. *An Introduction to Iterative Toeplitz Solvers*, SIAM: Philadelphia, 2007.

[37] G. Strang, A proposal for Toeplitz matrix calculations, *Studies in Applied Mathematics*, **2001,23(2), 494–510.**

[38] T. Chan, An optimal circulant preconditioner for Toeplitz systems, *SIAM Journal on Scientific and Statistical Computing*, **1988, 9, 766–771.**

[39] R. H. Chan, M. K. Ng, Conjugate gradient methods for Toeplitz systems,*SIAM Review* **, 1996, 38, 427–482.**

[40] M. Van Barel, G. Heinig, P. Kravanja, A stabilized superfast solver for nonsymmetric Toeplitz systems, *SIAM Journal on Matrix Analysis and Applications* **, 2001, 23, 494–510.**

[41] M. Stewart, A superfast Toeplitz solver with improved numerical stability, *SIAM Journal on Matrix Analysis and Applications*, **2003, 25, 669–693.**

[42] I. V. Oseletets, E. E. Tyrtyshnikov, A unifying approach to the construction of circulant preconditioners, *Linear Algebra and its Applications*, **2006, 435–449.**

Legends to Figures

1. Flapping elastic wing in the homogeneous flow of a non-viscous incompressible fluid.

2. Solution $|\gamma|$ versus variable x on the central chord of the wing ($y = 0$), for various number of nodes N: $\nu = 0.4$, $W(x, y) \equiv 1$.

3. Solution $|\gamma|$ versus variable y on the central wing-span line ($x = 0$), for various number of nodes N: $\nu = 0.4$, $W(x, y) \equiv 1$.

4. Solution $|\gamma|$ versus variable x on the central chord of the wing ($y = 0$), for various Strouhal number ν: $N = 4^9 = 262144$, $W(x, y) \equiv 1$.

5. A scaled-up fragment from Fig. 4.

6. Solution $|\gamma|$ versus variable y on the central wing-span line ($x = 0$), for various Strouhal number ν: $N = 4^9 = 262144$, $W(x, y) \equiv 1$.

7. Solution $|\gamma|$ versus variable y on the central wing-span line ($x = 0$), for various number of nodes N: $\nu = 0.4$, $W(x, y) = \cos(\pi y)$.

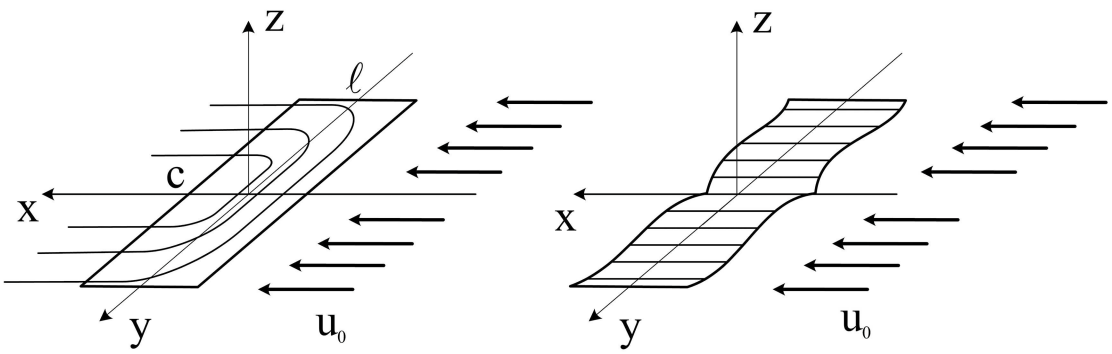

Fig. 1

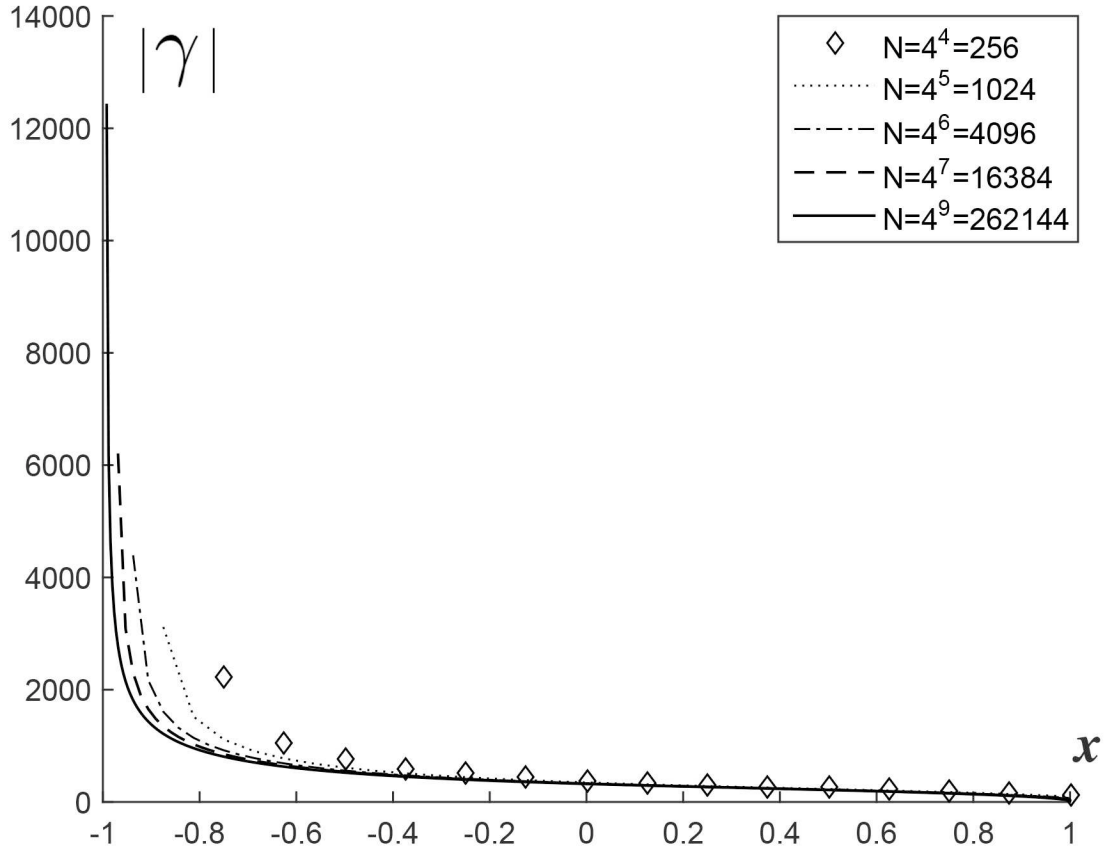

Fig. 2

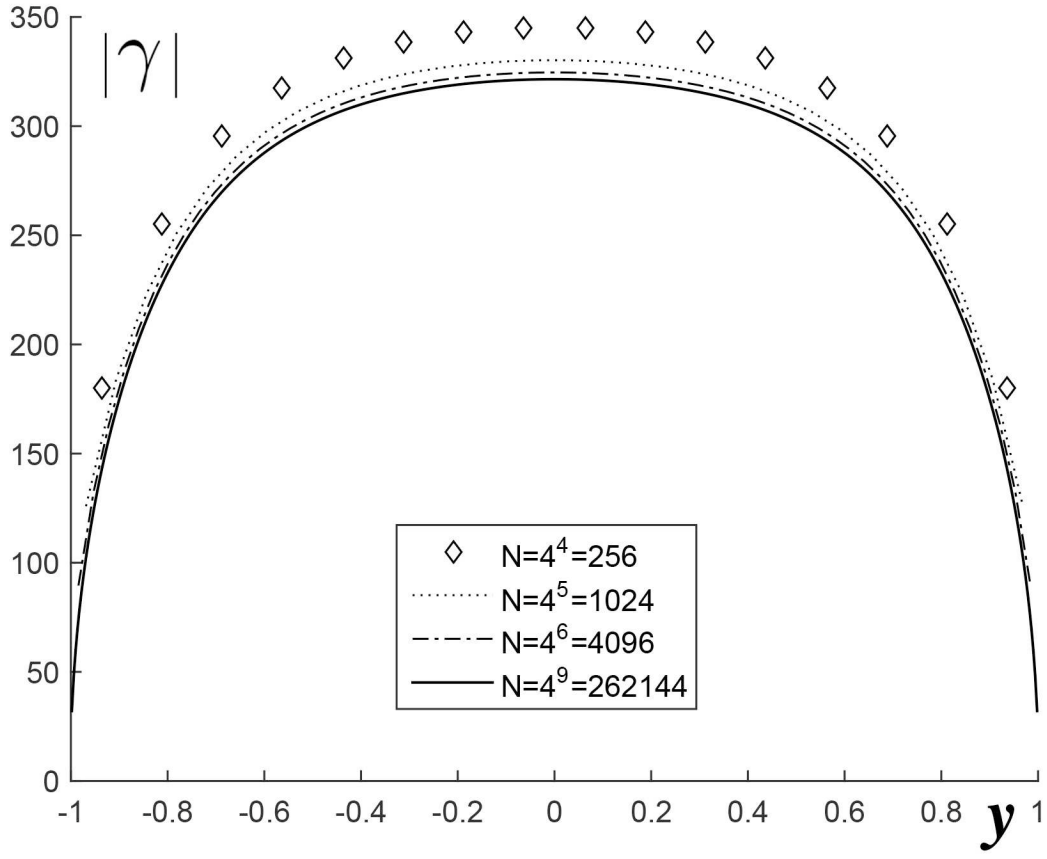
|γ|
350
300
250
200
150
100
50
0
-1
-0.8
-0.6
-0.4
-0.2
0
0.2
0.4
0.6
0.8
1
y
N=4^4=256
N=4^5=1024
N=4^6=4096
N=4^9=262144

Fig. 3

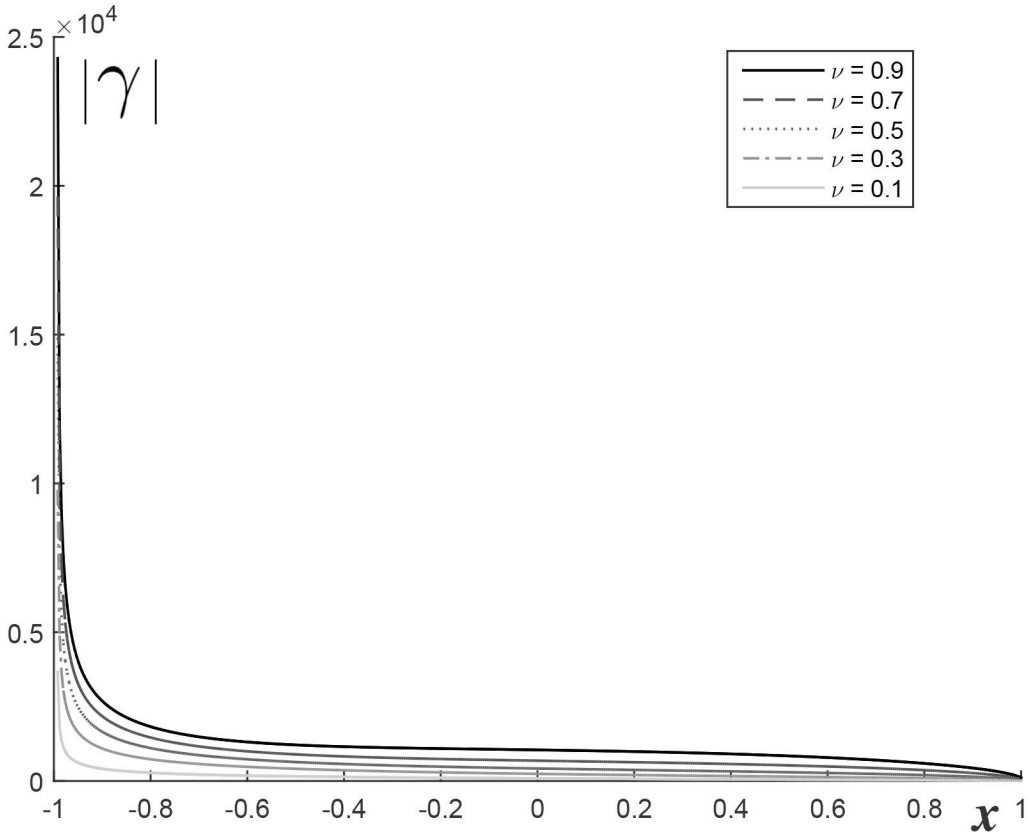

Fig. 4

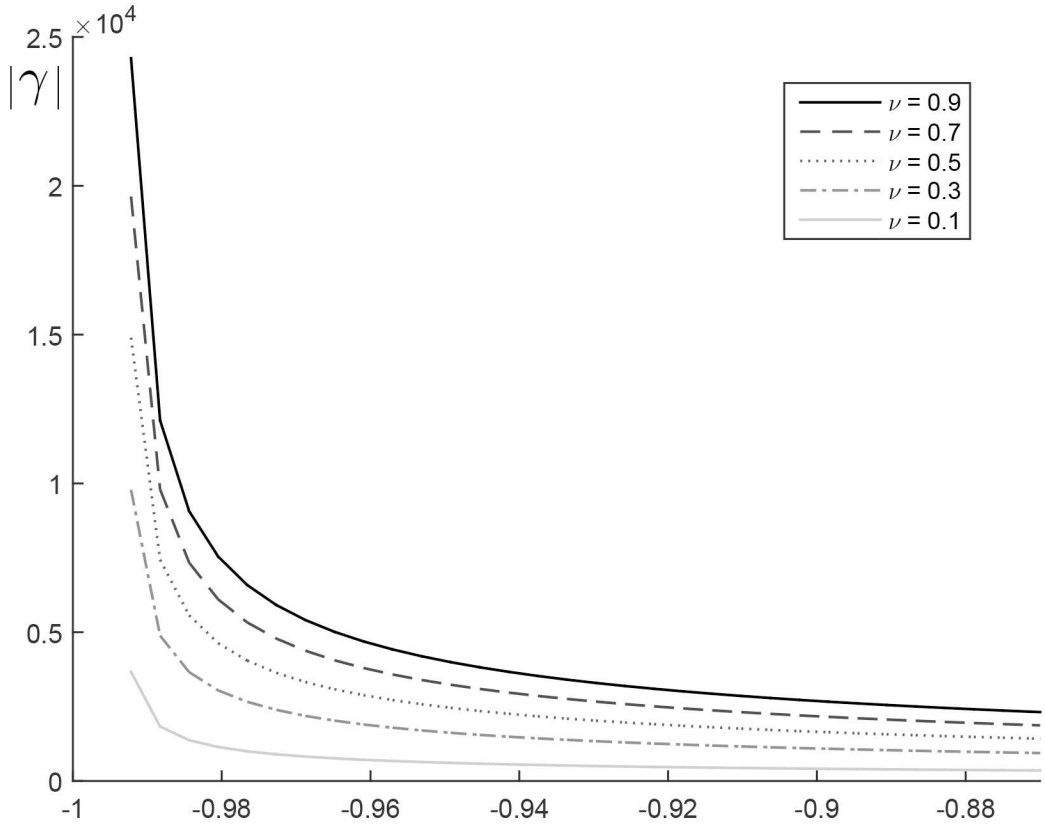

Fig. 5

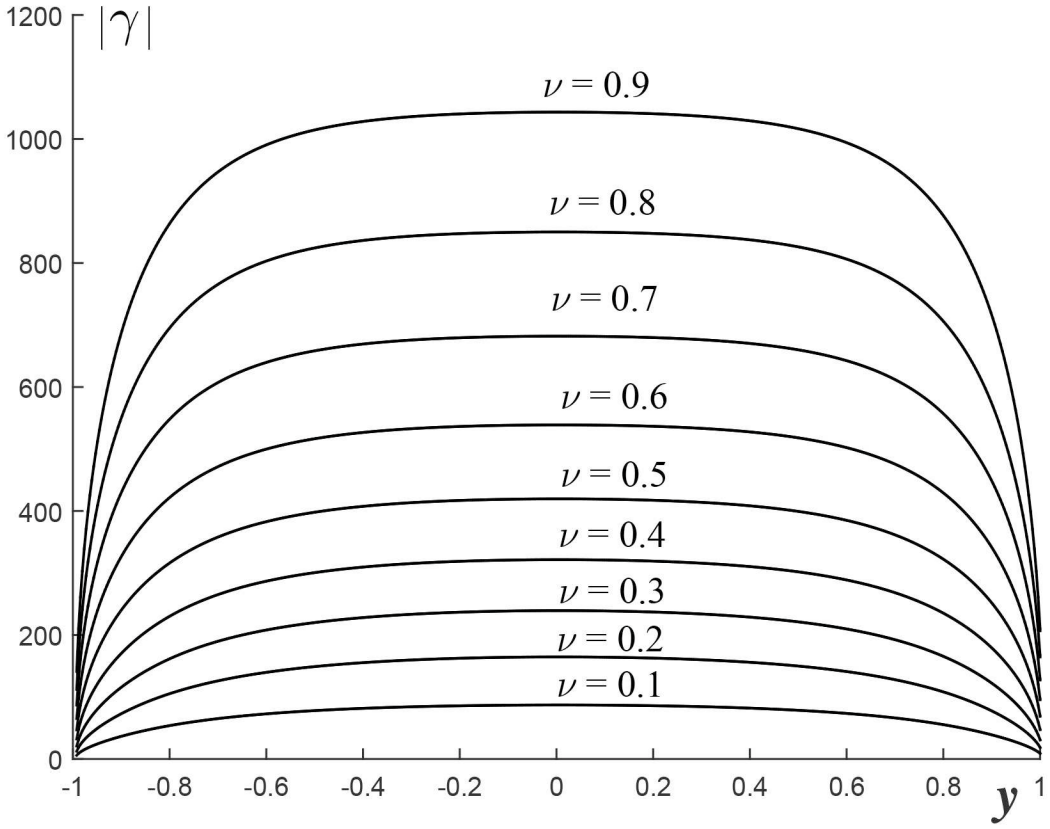

Fig. 6

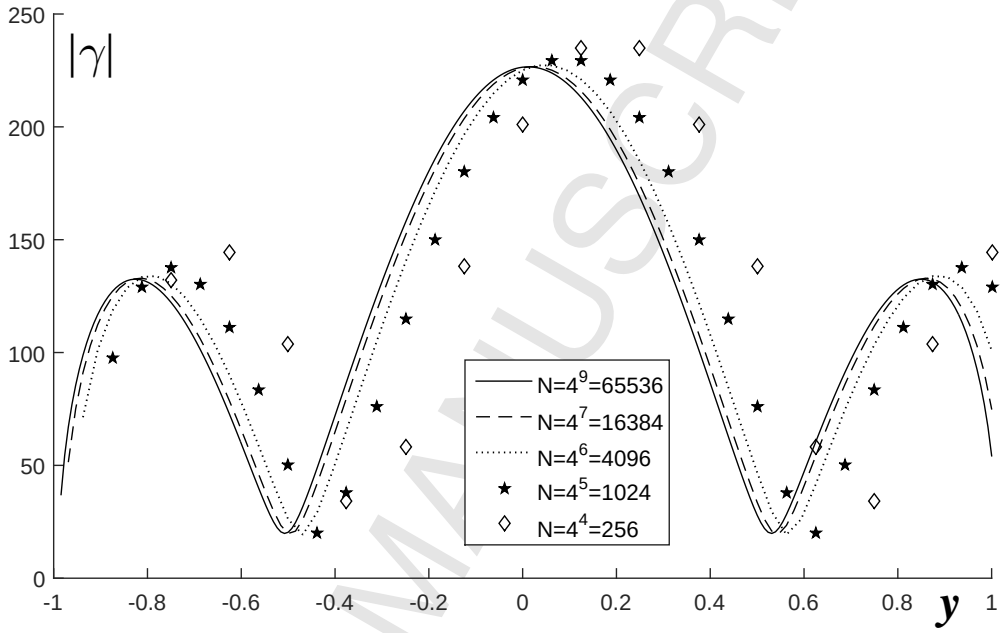

Fig. 7